Analyses and control of interphase structures and adhesion properties of epoxy resin/epoxy resin for development of CFRP adhesion systems

Aoki, Naho ; Yamazaki, Junpei ; Matsumoto, Takuya ; Totani, Masayasu ; Shundo, Atsuomi ; Tanaka, Keiji ; Nishino, Takashi

(Citation)
Composites Part A: Applied Science and Manufacturing,187:108511

(Issue Date)
2024-12

(Resource Type)
journal article

(Version)
Version of Record

Composites: Part A 187 (2024) 108511

Contents lists available at ScienceDirect

Composites Part A

journal homepage: www.elsevier.com/locate/compositesa

Analyses and control of interphase structures and adhesion properties of epoxy resin/epoxy resin for development of CFRP adhesion systems

Naho Aoki [a], Junpei Yamazaki [a], Takuya Matsumoto [a,*], Masayasu Totani [b], Atsuomi Shundo [b], Keiji Tanaka [b], Takashi Nishino [a,*]

[a] Department of Chemical Science and Engineering, Graduate School of Engineering, Kobe University, Rokko, Nada, Kobe 657-8501, Japan
[b] Department of Applied Chemistry, Kyushu University, Fukuoka 819-0395, Japan

ARTICLE INFO

Keywords:
Adhesion
Epoxy resin
Interphase
Confocal Raman spectroscopy

ABSTRACT

In the adhesion of carbon fiber reinforced plastics (CFRP), the boundary regions were composed of only epoxy resins of CFRP matrix and adhesives, and their similar epoxy structures pose significant difficulty in studying the adhesion mechanism. Herein, we focused on structure and properties of laminates of epoxy resin substrates and adhesives with different curing conditions of substrates. We prepared laminates using deuterated epoxy adhesives or fluorinated epoxy adhesives, and their boundary regions were identified through confocal Raman scattering measurements. The regions were distributed into "penetration" and "interphase". In particular, the penetration phase is a key of the adhesion properties. The penetration behaviors strongly depended on the crosslinking densities of the adherends, suggesting that the penetration regions would be directly impacted by the curing conditions of the substrates and molecular size of epoxy adhesive precursors. Our findings provide insights into novel designs of the reliable adhesion-based manufacturing systems of CFRP.

1. Introduction

In the automobile and aircraft industrial fields, carbon fiber reinforced plastics (CFRP) are the promising candidates as an alternative to metallic materials [1–3]. Because CFRP contain carbon fibers with high modulus and high strength in epoxy resin-based matrix, the density of CFRP is much lower than those of metallic materials. Therefore, the use of CFRP provides the effective decrease of vehicles weight and leads to lowering manufacturing costs, improving fuel efficiency, and promoting environmental preservation. In addition, the lightweight and excellent mechanical properties of CFRP provide numerous applications in various fields [4–6]. Actually, CFRP materials are employed in bumpers of automobiles, and main wings of aircrafts, as well as sport gears and repairing materials in bridges and buildings [7–9].

Manufacturing using adhesion technologies has been received much attention recently. In particular, adhesion of CFRP has larger advantages, relative to traditional material connection methods using bolts or rivets, because drilling or punching processes were not required and stress concentration was able to be avoided. The high strength and high modulus of CFRP are attributed to their aligned long carbon fibers. Therefore, drilling and punching processes for screwing and riveting in product manufacture lead to the decrease of the length of carbon fibers in CFRP and the deterioration of reinforcement effect of carbon fibers [10–12]. Furthermore, in contrast to the single point connection using screws and rivets, lamination and adhesion enable two-dimensional contact and provide stronger adhesion strength. For the wider spreading of CFRP materials, more developments of lamination and adhesion technologies are desired.

In adhesion of CFRP components, epoxy resin adhesives are conventionally employed. This reason is that epoxy resin possesses high mechanical strength, modulus and toughness, as well as high affinity toward the epoxy resin matrix in CFRP and simple coating and curing process leads to their credible adhesion properties. Epoxy resin / epoxy resin interface should be formed in the CFRP adhesion process. On the other hand, the reliable and concrete adhesion system has not completely established because adhesion strength and durability of CFRP were not sufficient. It is well-known that the adhesion of CFRP is a challenge because of their poor adhesion properties. Some adhesion systems of CFRP have been suggested by various researchers. For example, the dry surface modification such as plasma irradiation and electron beam irradiation introduce oxygen-based polar functional groups or reactive radical species to the polymer substrates [13–17] and

* Corresponding authors.
E-mail addresses: matsumoto0521@person.kobe-u.ac.jp (T. Matsumoto), tnishino@kobe-u.ac.jp (T. Nishino).

https://doi.org/10.1016/j.compositesa.2024.108511
Received 29 July 2024; Received in revised form 12 September 2024; Accepted 5 October 2024
Available online 9 October 2024

the wet surface modification through chemical reactions provides reactive functional groups to the substrates [5,18,19]. As one of the adhesion methods for the larger adhesion strength of CFRP, the control of the curing degree of the epoxy resin matrix in CFRP has been suggested. The CFRP substrates with unreacted epoxy groups conduct excellent adhesion properties through complete curing process after applying epoxy adhesives. This process is called as "co-curing" [20–24].

In the adhesion system of CFRP substrates, the analyses of interphase between epoxy resins are significant. However, the interphase with the same or similar chemical components has a huge obstacle to overcome. The interphase is not able to be distinguished chemically because of the same or similar chemical components at the interphase [25,26]. The network structures of epoxy resins have large impacts on not only their mechanical properties [27–29] but also their adhesion properties. In this work, we focused on the adhesion systems between epoxy resin substrates and epoxy resin adhesives and investigated on their adhesion interphase structures using deuterated epoxy resins and similar epoxy resins. In our previous reports and other groups' papers, it is proved that the adhesion boundary regions possess three-dimensional structure, namely "interphase", not two-dimensional interface [30–39]. Particularly, we evaluated the correlation among curing condition of epoxy resin substrates and adhesives, the thickness of interphase, and the adhesion properties. Through these evaluations, we clarified the mechanism and reason for the high adhesion strength between epoxy resins.

2. Experimental

2.1. Materials

In H-Epoxy resin, 2,2-bis(4-glycidyloxyphenyl) propane (Tokyo Chemical Industry Co., BADGE, epoxy equivalent: 170 g/eq) and jER®1001 (Mitsubishi Chemical Corporation, epoxy equivalent: 474 g/eq) were used as main epoxy precursors. 3- or 4-Hexahydro methyl phthalic anhydride (Combi blocks, or Angene International Limited, MHHPA) was used as a curing agent, and *N,N*-dimethylbenzylamine (Tokyo Chemical Industry Co., Ltd., DMBA) was used as a curing accelerator.

For the synthesis of deuterated bisphenol A diglycidyl ether (D-BADGE), deuterated bisphenol A (BPA-d_{14}, 98 %) and deuterated epichlorohydrin (EP-d_5, 98 %) purchased from Polymer Source Inc.) were used as starting reagents. Potassium hydroxide (Fujifilm Wako Co., KOH) and tetrabutylammonium bromide (Tokyo Chemical Industry Co., Ltd., TBAB) were used as a base and a phase transfer catalyst, respectively.

In F-Epoxy resin, fluorinated epoxy precursor (Mitsubishi Chemical Corporation, jER® YX7760, epoxy equivalent: 235 g/eq) was used as a main agent, MHHPA was used as a curing agent, and 2-ethyl-4-methylimidazole (Tokyo Chemical Industry Co., Ltd., 2E4MZ) was used as a curing accelerator.

All chemicals were used without any purification. Their chemical structures of BADGE and D-BADGE are shown in Fig. 1. These epoxy reagents were used for the component detection in the interphse of the laminate speciemens in the confocal Raman spectroscopy.

2.2. Preparation of epoxy substrates

2.2.1. Synthesis of D-BADGE

In a round-bottomed flask, BPA-d_{14} (9.78 g, 40.3 mmol) was dissolved in EP-d_5 (20.1 mL, 247 mmol), followed by the addition of KOH (3.48 g, 62.0 mmol) and TBAB (1.63 g, 5.06 mmol). The reaction solution was then stirred overnight at room temperature under nitrogen atmosphere. Water was added into the solution, the resulting in the phase separation, and then the organic phase was collected. The organics in the residual water phase were extracted twice with diethyl ether. All the organic phases including diethyl ether one were combined and then washed with water. The organic phase was dried with sodium sulfate, filtered and evaporated. The crude product was purified by silica chromatography eluted with a mixture of *n*-hexane/ethyl acetate (2:1). The solvent was evaporated to produce a slightly yellowish liquid with a yield of 12.4 g (84 %). The chemical structure of the product was characterized using carbon-nuclear magnetic resonance (^{13}C NMR) spectroscopy (JNM-ECZ400 NMR spectrometer, JEOL Ltd.). ^{13}C NMR (400 MHz, DMSO-d_6): δ = 29.5–31.0 ppm (br), 40.7–41.0 ppm (m), 43.1–43.7 ppm (m), 48.9–49.5 ppm (m), 68.1–68.8 ppm (m), 113.3–113.8 ppm (m), 126.9–127.3 ppm (m), 142.7 ppm (s), 156.0 ppm (s).

2.2.2. Preparation of H-Epoxy substrates

The H-Epoxy precursor, BADGE, was mixed with MHHPA and DMBA at 40 °C. The ratios of MHHPA/BADGE and DMBA/ BADGE were 1 w/w and 0.01 w/w, respectively. After stirring for 30 min and degassing for 60 min under vacuum at 40 °C, the mixture was first cured at 100 °C for 30 min. The final curing was conducted at 110 °C, 120 °C, and 140 °C for 2 h to obtain H-Epoxy-110, H-Epoxy-120, and H-Epoxy-140 substrates, respectively. The thickness of their substrates in laminate films were around 300 μm for Raman scattering measurements and 600 μm for wedge tests. Their prepared substrates are summarized in Table 1.

2.2.3. Preparation of fluorinated-Epoxy (F-Epoxy) substrates

Also, as shown in Table 1, the F-Epoxy precursor (YX7760) was mixed with MHHPA and 2E4MZ at 80 °C. The ratios of MHHPA/YX7760 and 2E4MZ/ YX7760 were 0.71 w/w and 0.005 w/w, respectively. After stirring for 30 min and degassing for 15 min under vacuum at 80 °C, the mixture was first cured at 100 °C for 20 min. The final curing was conducted at 110 °C and 140 °C for 2 h to obtain F-Epoxy-110 and F-Epoxy-140, respectively. The thickness of their substrates in the laminate films was around 300 μm for Raman scattering measurements and 600 μm for wedge tests.

Table 1
Preparation details of epoxy substrates.

Substrate	Main agent	Curing agent	Accelerator	Curing condition
H-Epoxy-110	BADGE	MHHPA	DMBA	110 °C, 2 h
H-Epoxy-120				120 °C, 2 h
H-Epoxy-140				140 °C, 2 h
F-Epoxy-110	YX7760	MHHPA	2E4MZ	110 °C, 2 h
F-Epoxy-140				140 °C, 2 h

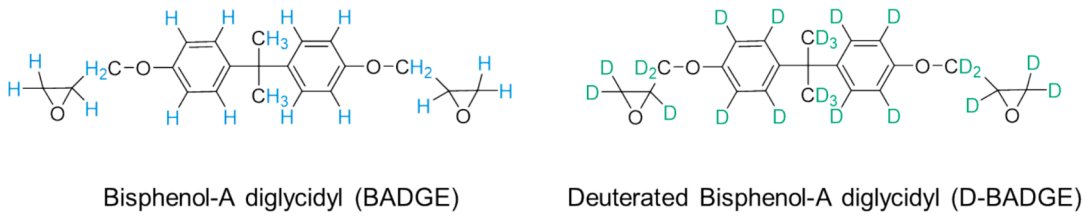

Fig. 1. Chemical structure of BADGE and D-BADGE.

2.3. Preparation of samples for Raman scattering spectroscopy

The laminate samples prepard for Raman scattering spectroscopic measurement were summarized in Table 2.

2.3.1. Preparation of D-Epoxy/H-Epoxy laminate film

D-Epoxy/H-Epoxy laminates were prepared by applying and curing the mixture including D-Epoxy precursor on H-Epoxy substrates. MHHPA and DMBA were added into D-Epoxy precursor at 40 °C and stirred for 30 min. The weight ratios of MHHPA and DMBA for D-Epoxy precursor were 0.92 w/w and 0.01 w/w, respectively. The mixtures were applied onto H-Epoxy substrates (H-Epoxy-110, H-Epoxy-120, and H-Epoxy-140) and all the samples were cured at 140 °C for 2 h, and D-H-110, D-H-120, and D-H-140 were obtained, respectively, as shown in Table 2.

2.3.2. Preparation of F-Epoxy/H-Epoxy laminate films

F-Epoxy/H-Epoxy laminates, F-H-110 or F-H-140, were prepared by applying and curing the mixture including F-Epoxy precursor on H-Epoxy substrates. MHHPA and 2E4MZ were added into YX7760 at 80 °C and degassed for 15 min. The weight ratios of MHHPA and 2E4MZ for epoxy main agent YX7760 were 0.71 w/w and 0.005 w/w, respectively. The mixtures were applied onto H-Epoxy plates (H-Epoxy-110 and H-Epoxy-140), and the samples were cured at 140 °C for 2 h, and F-H-110 or F-H-140 were obtained, respectively.

2.3.3. Preparation of H-Epoxy/F-Epoxy laminate film

As shown in Table 2, H-Epoxy/F-Epoxy laminates were prepared by applying and curing the mixture including BADGE and JER®1001 on F-Epoxy substrates. The weight fraction of BADGE and jER®1001 in the epoxy precursor mixtures were 100/0, 50/50, and 0/100, for $\phi = 100$ %, 50 % and 0 %, respectively. Before adding the curing agent and accelerator, the epoxy mixtures were stirred for 30 min at 40 °C for $\phi = 100$ %, 90 °C for $\phi = 50$ %, and 100 °C for $\phi = 0$ %, respectively. The stirring temperatures were optimized because of melting temperatures of the main agents. MHHPA and DMBA were added into the mixtures at the stirring temperatures. The weight ratios of MHHPA and DMBA for epoxy precursors were 1 w/w and 0.003 w/w for $\phi = 100$ %, 0.52 w/w and 0.003 w/w for $\phi = 50$ %, 0.35 w/w and 0.003 w/w for $\phi = 0$ %, respectively. The mixtures were applied onto F-Epoxy-110 and F-Epoxy-140, and all the samples were cured at 140 °C for 2 h, and H-F-$110_{\phi100}$, H-F-$110_{\phi50}$, H-F-$110_{\phi0}$, H-F-$140_{\phi100}$, H-F-$140_{\phi50}$ and H-F-$140_{\phi0}$ were obtained, respectively.

Table 2
Fabricated laminated samples for Raman scattering spectroscopy and wedge tests.[5]

Sample Name	Substrate	Epoxy laminated or sandwiched	Raman	Wedge test
D-H-110	H-Epoxy-110	D-Epoxy	✓	—
D-H-120	H-Epoxy-120		✓	—
D-H-140	H-Epoxy-140		✓	—
H-H-110	H-Epoxy-110	H-Epoxy $\phi = 100$ %	—	✓ (H-H-H-110)
H-H-120	H-Epoxy-120	H-Epoxy $\phi = 100$ %	—	✓ (H-H-H-120)
H-H-140	H-Epoxy-140	H-Epoxy $\phi = 100$ %	—	✓ (H-H-H-140)
F-H-110	H-Epoxy-110	F-Epoxy	✓	✓ (H-F-H-110)
F-H-140	H-Epoxy-140		✓	✓ (H-F-H-140)
H-F-$110_{\phi100}$	F-Epoxy-110	H-Epoxy $\phi = 100$ %	✓	✓ (F-H-F-110)
H-F-$110_{\phi50}$		H-Epoxy $\phi = 50$ %	✓	—
H-F-$110_{\phi0}$		H-Epoxy $\phi = 0$ %	✓	—
H-F-$140_{\phi100}$	F-Epoxy-140	H-Epoxy $\phi = 100$ %	✓	✓ (F-H-F-140)
H-F-$140_{\phi50}$		H-Epoxy $\phi = 50$ %	✓	—
H-F-$140_{\phi0}$		H-Epoxy $\phi = 0$ %	✓	—

2.3.4. Preparation of cross section samples for Raman scattering measurements

The cross sections of the laminate films embedded in epoxy resin were fabricated using an ultra-microtome (Leica microsystems, EM UC6) with a diamond knife (Symtek Co., Ltd, SYMX3055).

2.4. Preparation of specimens for wedge tests

The laminate samples prepard for wedge tests were summarized in Table 2.

2.4.1. Preparation of H-H-H laminates

In order to investigate the adhesion strength between the same epoxy resin, wedge tests for the adhesion samples between H-Epoxy/H-Epoxy substrates are performed, as shown in Figure S2 in the Supplementary material.

The H-Epoxy precursors of BADGE/MHHPA/DMBA were coated on H-Epoxy substrates, H-Epoxy-110, H-Epoxy-120 or H-Epoxy-140. The thickness of the coated H-Epoxy resin was 50 μm. Another H-Epoxy substrate was placed onto this adhesive coating on the substrate and cured at 140 °C for 2 h. Each sandwiched sample was trimmed into a rectangle of 10 mm × 40 mm. For wedge test samples, H-H-H adhered laminates based on H-Epoxy-110, H-Epoxy-120, and H-Epoxy-140 substrates were obtained as H-H-H-110, H-H-H-120 and H-H-H-140, respectively.

2.4.2. Preparation of H-F-H laminates

The adhered samples for wedge tests in Figure S2 in the Supplementary material were prepared. The F-Epoxy precursors of YX7760/MHHPA/2E4MZ were coated on a H-Epoxy substrate, H-Epoxy-110 or H-Epoxy-140. The thickness of the coated F-Epoxy resin was 50 μm. Another H-Epoxy substrate was placed onto this adhesive coated on the substrate and cured at 140 °C for 2 h. Each sandwiched sample was trimmed into a rectangle of 10 mm × 40 mm. For wedge test samples, H-F-H adhered laminates were obtained as H-F-H-110 ad H-F-H-140, respectively.

2.4.3. Preparation of F-H-F laminates

The H-Epoxy precursors of BADGE/MHHPA/DMBA were coated on a F-Epoxy substrate (F-Epoxy-110 and F-Epoxy-140). The thickness of the coated H-Epoxy resin was 50 μm. Another F-Epoxy substrate was placed onto this adhesive coated on the substrate and cured at 140 °C for 2 h. Each sandwiched sample was trimmed into a rectangle of 10 mm × 40 mm. For wedge test samples, F-H-F adhered laminates based on F-Epoxy-110 and F-Epoxy-140 substrates were obtained, as F-H-F-110 and F-H-F-140, respectively.

2.5. Thermal analyses of Epoxy substrate

In order to investigate on the curing degree at various curing temperatures, thermal analyses with a differential scanning calorimeter (DSC, Rigaku Corporation, DSC8230) were performed for H-Epoxy substrates cured at 100 °C, 110 °C, 120 °C and 140 °C, and F-Epoxy substrates cured at 110 °C, 140 °C, 150 °C, 160 °C, 170 °C and 180 °C. All measurements were carried out under N_2 at a heating rate of 5 °C/min from room temperature to 200°C, using Al pans. The flow rate of N_2 gas was 70 mL/min.

2.6. Raman scattering measurement

Raman scattering spectra of H-Epoxy, D-Epoxy, and F-Epoxy

substrates were measured in a single spot mode using a confocal Raman spectroscope (WITec, Alpha 300R). Nd/YAG semiconductor was used as a laser source with an excitation wavelength of 532 nm and an intensity of 20 mW. The magnification of objective lens with numerical aperture of 0.75 was 50. The exposure time was 0.5 s, the accumulation was 10 times, and the diffraction grating was 600 gr/mm.

Line scanning measurements were also employed to estimate the interphase thickness of the prepared laminates. Raman scattering spectra across the interphase of the cross section of laminates were measured by step-by-step scanning with around 300 nm intervals, as shown in Figure S3 in the Supplementary material. The spatial resolution in the in-plane direction d_{xy} was defined by the following Rayleigh's equation (1):

$$d_{xy} = k\lambda/NA \tag{1}$$

where k is 0.61 for this apparatus,λ is wavelength, and NA is numerical aperture of the objective lens. The value of d_{xy} was 433 nm. In a line scanning measurement, the intervals between Raman scattering measurement points were around 300 nm.

2D mapping measurements were performed using the same apparatus. The magnification of objective lens with numerical aperture of 0.75 was 50 times, the exposure time was 0.1 s, the accumulation was 1 time, the scanning area was 20 μm × 30 μm for D-H-110, 20 μm × 20 μm for D-H-140, respectively, and the distance between the stepping points was around 300 nm. The 2D images were plotted using the intensity of CD_2 stretching bands at around 2293 cm^{-1} [40,41].

In the line scanning and 2D mapping measurements, the focal points were adjusted to the surface of the cross section of the samples.

2.7. Energy dispersion spectroscopy (EDS) observation

The interphase structures of the cross-section of the laminate films, F-H-110 and F-H-140 were observed by energy dispersion spectroscopy (EDS, JEOL Ltd., JED-2300) equipped on a field-emission scanning electron microscope (FE-SEM, JEOL Ltd., JSM-7100F). Osmium was sputtered on the cross-section samples before observation. The emission current was 8nA, the acceleration voltage was 15 kV and the magnifications were 4000. The accumulation times in the EDS measurement were 100.

2.8. Dynamic mechanical analysis (DMA) and crosslinking density

Dynamic storage modulus (*E'*) and mechanical loss tan δ were measured using a dynamic mechanical analyzer (ITK Co, Ltd., DVA-220S) from room temperature to 250 °C. The samples were trimmed into 5 mm × 30 mm of rectangles. The heating rate was 6 °C /min, the initial length was 20 mm, and the frequency was 4 Hz. The crosslinking density was calculated by following equation (2) [42].

$$\nu = \frac{E'}{3RT} \tag{2}$$

where ν is crosslinking density (mol/m^3), *E'* is storage modulus at T_g + 30 K (Pa), *T* is absolute temperature (K), *R* is Gas constant (8.31 J/mol·K).

2.9. Symmetric wedge tests of the adhered specimens

The adhesive strengths of the epoxy laminates were evaluated based on the fracture toughness G_c measured by wedge tests. In the wedge test, a single-edged razor blade with a thickness of 76 μm was inserted at the adhesive layer region until the edge of the razor blade achieved to 10 mm from the sample edge. The crack propagation length *a* between the edge of the blade and the crack tip was measured using an optical microscope (HIROX Co., Ltd.) 24 h after the insertion. Then, the blade was further inserted two times by 5 mm for each insertion. The propagation length *a* were measured 24 h, 48 h and 72 h after wedging, and the values of *a* were averaged. The propagation length of each sample was measured for more than 3 specimens. The fracture toughness G_c was calculated by the following equation (3) [43].

$$G_c = \frac{3b^2Ed^3}{16a^4\left(1+\frac{0.64d}{a}\right)^4} \tag{3}$$

where *b* is the thickness of the razor blade, *E* is the Young's modulus of epoxy substrate, and *d* is the average thickness of epoxy substrate. *E* was evaluated by a stress–strain curve using a tensile tester (AUTOGRAPH AG-X plus, Shimadzu Co.) at a crosshead speed of 0.5 mm/min at room temperature. The sample size was 5 mm × 40 mm, and the initial length was 20 mm.. The Young's modulus of over 5 specimens were averaged for each sample.

3. Results and discussion

3.1. Curing reaction progress by thermal analyses

To investigate on the progress degrees of curing reaction of epoxy substrates, DSC measurements were performed. Figures S4 (a) and (b) in the Supplementary material show the DSC thermograms of H-Epoxy and F-Epoxy substrates with various curing temperatures. The progress of curing reaction of epoxy resin was evaluated. H-Epoxy samples were cured at 100 °C and 110 °C in Figure S4(a), and F-Epoxy samples were cured at 110 °C, 140 °C and 150 °C in Figure S4(b), In their DSC curves, broad exothermic peaks were observed. These results suggested that the curing reactions in their epoxy substrates had not been completed at their curing temperatures. With the increases of the curing temperature of the H-Epoxy and the F-Epoxy substrates, the exothermic peaks decreased. In the H-Epoxy cured at 140 °C and in the F-Epoxy cured at 160 °C, 170 °C and 180 °C, the peaks of the curing reaction disappeared. This implied that the curing reactions of H-Epoxy at 140 °C and F-Epoxy at 160 °C, 170 °C and 180 °C were completed. Unfortunately, in the substrates of both the epoxy resins cured at a temperature higher than 140 °C, fluorescences were observed in Raman scattering measurements. In this case, Raman scattering spectra could not be obtained to evaluate the interphase structure in epoxy substrates. Therefore, H-Epoxy and F-Epoxy cured from 110 °C to 140 °C were employed as adherent substrates in this study.

3.2. Raman scattering measurement

3.2.1. Single spot Raman scattering measurement

As shown in Figure S5 in the Supplementary material, in the Raman spectrum of H-Epoxy, two characteristic band peaks were observed at 1116 and 3070 cm^{-1}, which were assigned to the vibration bands of CH of aromatic ring and CH_2 of epoxide, respectively [44]. In the Raman spectrum of D-Epoxy, defined band peaks were observed at around 2293 cm^{-1} originated from CD_2 vibration [40,41]. In contrast, no band peak in Raman scattering spectrum of H-Epoxy substrate was observed at around 2293 cm^{-1}. In the case of interphase evaluation of H-Epoxy/D-Epoxy adhered specimens, we focused on the bands at 3070 cm^{-1} and 2293 cm^{-1}.

On the other hand, in the Raman spectrum of F-Epoxy, a defined band peak was observed at 1178 cm^{-1}, which would be attributed to CF_3 groups [45]. In addition, no band peak in Raman scattering spectrum of the cured H-Epoxy substrates was observed at around 1178 cm^{-1}. In the case of evaluation of interphase of H-Epoxy/F-Epoxy adhered specimens, we focused on the intensities of their characteristic bands at 1116 cm^{-1} and 1178 cm^{-1}.

We succeeded to distinguish the epoxy resins with same structure spectroscopically, H-Epoxy and D-Epoxy, by Raman scattering measurement using deuterated epoxy resin. In addition, we could also distinguish H-Epoxy and F-Epoxy with similar structure by focusing on

above bands. The Raman scattering measurement take large advantages in evaluation of the interphase between same or similar epoxy materials.

3.2.2. Line scanning Raman scattering measurement

We performed Raman scattering measurements of the cross sections of the epoxy laminates along lines across their interphases with around 300 nm intervals. Fig. 2 (a) and (b) show Raman spectra of D-H-140 and F-H-140 scanned across the interphase from H-Epoxy to D-Epoxy side, and from H-Epoxy to F-Epoxy side, respectively.

In H-Epoxy/D-Epoxy adhered specimens, D-H-110, D-H-120 and D-H-140 samples, as the measurement positions moved across the interphase from H-Epoxy side to D-Epoxy side, the band peaks of H-Epoxy at 3070 cm^{-1} gradually disappeared, whereas the band intensities of D-Epoxy substrates at 2293 cm^{-1} were increased. At the interphase, both the bands of H-Epoxy and D-Epoxy components were observed and their component ratios were inverted. The inverting regions were composed of both the components of H-Epoxy and D-Epoxy.

In H-Epoxy/F-Epoxy adhered specimens, F-H-110 and F-H-140, as the measurement positions moved across the interphase from H-Epoxy side to F-Epoxy side, the bands of H-Epoxy substrates at 1116 cm^{-1} gradually disappeared, whereas the band intensities of F-Epoxy substrates at 1178 cm^{-1} emerged. At the interphase, both the band intensities of H-Epoxy and F-Epoxy components were inverted and, in the inverting regions, both the components of H-Epoxy and F-Epoxy were also detected.

Fig. 3 (a), (b) and (c) show the plots of relative intensities of their defined peaks at every measurement position in D-H-110, D-H-120 and D-H-140, respectively. The relative intensity $I_{D/H}$ was calculated with the following equation (4) based on the intensities of 3070 cm^{-1} and 2293 cm^{-1} for I_H and I_D, respectively.

$$I_{D/H} = \frac{I_D}{I_D + I_H} \tag{4}$$

Figures S6 (a) and (b) in the Supplementary material show the plots of relative intensities of their defined peaks at every measurement position in F-H-110 and F-H-140 samples, respectively. The relative intensity was calculated with following equation (5) based on the intensities of 1116 cm^{-1} and 1178 cm^{-1} for I_H and I_F, respectively.

$$I_{F/H} = \frac{I_F}{I_F + I_H} \tag{5}$$

3.2.3. Interphase of D-H-110, D-H-120 and D-H-140 samples

As shown in Fig. 3 (a), (b) and (c), as the measurement positions moved across the interphase from H-Epoxy side to D-Epoxy side, the $I_{D/H}$ of D-H-110, D-H-120 and D-H-140 were gradually and then abruptly increased. This result implied that the interphase was able to be detected spatially by confocal Raman scattering microspectroscopy using deuterated epoxy resin. The interphase of D-Epoxy/H-Epoxy samples was regarded as a typical model of the "interphase" with the same components [38,39]. In addition, the region with the increase of the relative intensity was divided into two phases in all the D-Epoxy/H-Epoxy adhered samples. The gradual-increasing regions were defined as "penetration", and the abrupt-rising regions were defined as

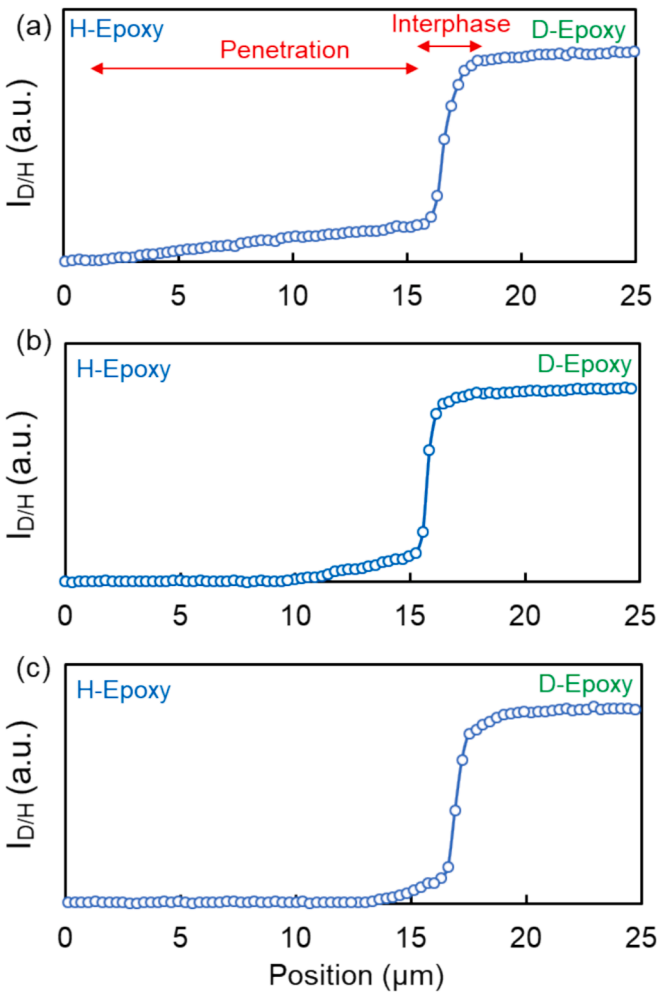

Fig. 3. Intensity distribution $I_{D/H}$ of Raman bands across the interphase of (a) D-H-110, (b) D-H-120 and (c) D-H-140.

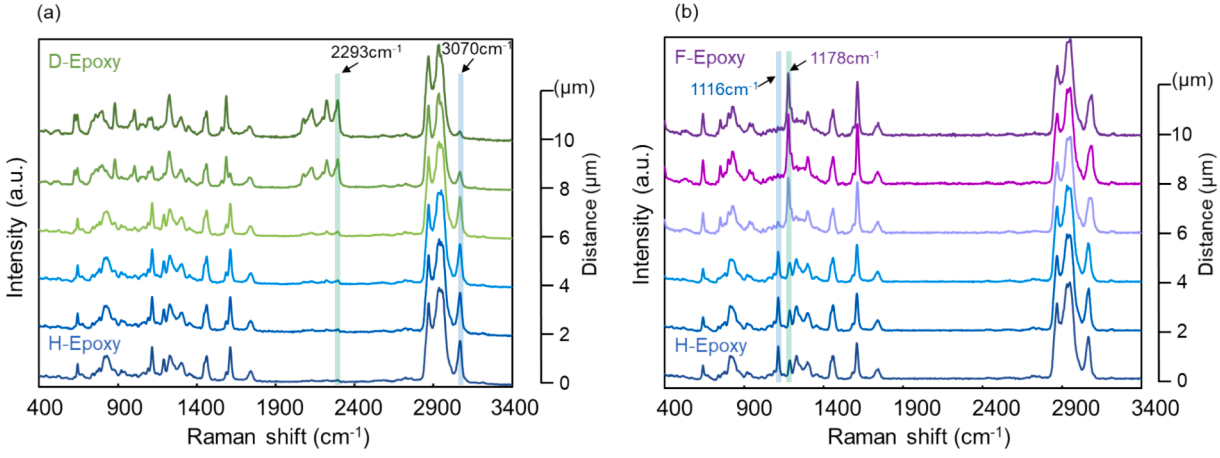

Fig. 2. Raman scattering spectra across the interphase of (a) D-H-140 and (b) F-H-140.

"interphase". For clear identification, their regions were characterized from differential intensities plots, as shown in Figure S7 in the Supplementary material. The region with the sharp peak was regarded as "interphase", and the "penetration" region was defined as that with slight increase of the diffrentail intensities. Both the thicknesses are summarized in Table 3. The interphase thicknesses were 2.9 μm for D-H-110, 2.9 μm for D-H-120, and 3.5 μm for D-H-140. There was no significant difference in their interphase thicknesses. In contrast, the penetration thicknesses were 14.5 μm for D-H-110, 5.6 μm for D-H-120, and 3.5 μm for D-H-140. As the curing temperature of the H-Epoxy substrates increased from 110 °C to 140 °C, the penetration thickness was decreased clearly. These results suggested that the curing temperature of the substrates had a more significant effect on the penetration region than on the interphase region.

In Fig. 4, the correlation between the thicknesses of penetration and interphase regions and their total thicknesses of D-H-110, D-H-120, and D-H-140 samples were summarized. The thickness of the penetration region decreased as the curing temperature of the H-Epoxy substrates increased, whereas no significant difference in interphase thickness was observed. Their total thickness depended more on their penetration region rather than on the interphase region in all the D-Epoxy/H-Epoxy adhered samples.

As shown in Fig. 5 and Figure S8 in the Supplementary material, we performed confocal Raman 2D mapping measurements of cross section of D-H-110 and D-H-140. The 2D mapping images were based on the CD_2 absorption band intensities at 2293 cm^{-1} around the interphase of D-H-110 and D-H-140. In their 2D mapping images, their interphases between H-Epoxy and D-Epoxy resins were visualized. As the curing temperature of the substrates increased from 110 °C to 140 °C, the contrast around their interphase was increased and the interphase region was narrowed. These results were coincident with those of their line scanning measurements.

3.2.4. Interphase of F-H-110 and F-H-140 samples

The relative intensities $I_{F/H}$ of F-H-110 and F-H-140 were plotted in Figures S6 in the Supplementary material. As the measurement positions moved across the interphase from H-Epoxy side to F-Epoxy side, $I_{F/H}$ of F-H-110 and F-H-140 were inceased gradually, followed by an abrupt rise. This result suggested that the interphase was able to be detected spatially by confocal Raman scattering microspectroscopy in spite of their similar chemical structure. In addition, the relative intensity increases were divided into "penetration" and "interphase" regions in all the F-Epoxy/H-Epoxy adhered samples. These thicknesses were also summarized in Table 3. The interphase thickness was 2.5 μm for F-H-110 and 2.6 μm for F-H-140. In contrast, the penetration thickness was 7.4 μm for F-H-110 and 2.6 μm for F-H-140. As the curing temperature of H-Epoxy substrates increased from 110 °C to 140 °C, only the penetration thickness was decreased. This result indicated that a lower curing temperature of the adherent substrates enhanced the expansion of the penetration region.

In Figures S9 (a) and (b) in the Supplementary material, the element mapping images with SEM-EDS and the plots of their element distribution around the interphase of F-H-110 and F-H-140 adhered samples were shown. In their EDS images, the interphase was detected because only the F-Epoxy included fluorine groups. The border regions between F-Epoxy and H-Epoxy substrates were distinguished clearly as the interphase regions, and the blurred parts were observed as penetration regions. In their distribution plots, F-H-110 samples possessed the larger penetration region, relative to F-H-140. As the curing temperature of substrate increased from 110 °C to 140 °C, their penetration regions were narrowed. These results supported the change of the penetration thickness in confocal Raman scattering measurements.

In addition, compared with D-Epoxy/H-Epoxy and F-Epoxy/H-Epoxy systems, penetration thicknesses of D-H-110 and F-H-110 were 14.5 μm and 7.4 μm, and D-H-140 and F-H-140 were 3.5 μm and 2.6 μm, respectively. The penetration thicknesses of D-Epoxy/H-Epoxy were larger compared with F-Epoxy/H-Epoxy for both the substrates cured at 110 °C and 140 °C. This suggested that the diffusion of molecules with the same chemical structures was more enhanced than that of the molecules with similar but different chemical structures.

3.2.5. Interphase of H-F-110$_{\phi100}$, H-F-110$_{\phi50}$, H-F-110$_{\phi0}$, H-F-140$_{\phi100}$, H-F-140$_{\phi50}$, and H-F-140$_{\phi0}$ samples

Next, we focused and investigated on the effect of the molecular size of epoxy precursors on the adhesion interphase structure using BADGE and jER®1001 with the same chemical structures but different molecular weights. The molecular weights were 340 and 948 for BADGE and jER®1001, respectively. The H-Epoxy adhesives with the BADGE/jER®1001 wt fractions of 100/0, 50/50 and 0/100 were prepared and their fractions of BADGE were represented as ϕ100, ϕ50 and ϕ0, respectively. Figures S10 (a)-(c) show the intensity distribution plots of Raman bands across the interphase between H-Epoxy and F-Epoxy in H-F-110$_{\phi100}$, H-F-110$_{\phi50}$, and H-F-110$_{\phi0}$ samples. In their distribution plots of Raman scattering band intensities, the penetration and interphase regions were also assigned. Their thicknesses are summarized in Table 4. The penetration thickness was 9.6 μm for H-F-110$_{\phi100}$, 2.8 μm for H-F-110$_{\phi50}$, and 1.1 μm for H-F-110$_{\phi0}$. The interphase thickness was 3.3 μm for H-F-110$_{\phi100}$, 3.4 μm for H-F-110$_{\phi50}$, and 2.1 μm for H-F-110$_{\phi0}$. As the weight ratio of BADGE in the epoxy mixtures was decreased from 100 % to 0 %, only the penetration thickness, not the interphase thickness, was decreased significantly. These reasons are that the smaller molecules of BADGE would be diffused and penetrated more rapidly in the network structure of F-Epoxy, relative to larger jER®1001. These results indicated that the penetration thickness depended on the averaged molecular size of the epoxy precursors, and larger molecules of the epoxy precursor prevents the diffusion into the epoxy substrate.

Figure S11 in the Supplementary material summarizes the thicknesses of penetration and interphase regions and the total thickness of H-F-110$_{\phi100}$, H-F-110$_{\phi50}$, H-F-110$_{\phi0}$, H-F-140$_{\phi100}$, H-F-140$_{\phi50}$, and H-F-140$_{\phi0}$. For the F-Epoxy-140 substrates cured at 140 °C, the penetration thickness was 3.2 μm for H-F-140$_{\phi100}$, 1.5 μm for H-F-140$_{\phi50}$, and 1.2 μm for H-F-140$_{\phi0}$. The interphase thicknesses were 3.2 μm for H-F-140$_{\phi100}$, 2.6 μm for H-F-140$_{\phi50}$, and 2.3 μm for H-F-140$_{\phi0}$. The largest molecular precursor with $\phi = 0$ % showed the lowest penetration thickness. This dependence of the penetration thickness of H-F-140 adhesion samples on averaged molecular size of H-Epoxy precursors was corresponding to the result of H-F-110 samples. In addition, as the curing temperature increased from 110 °C to 140 °C, the penetration thickness decreased for all F-Epoxy samples.

3.3. Cross linking densities of the epoxy adherents

For the investigation on the crosslinking densities of the epoxy network structures in the adherents, we performed DMA measurements of the cured epoxy substrates.

Figures S12 (a)-(d) in the Supplementary material show the temperature dependence of the storage modulus (É) and the crosslinking density (ν) for H-Epoxy-110, H-epoxy-120, H-Epoxy-140, F-Epoxy-110 and F-Epoxy-140. The ν was calculated from the É at higher temperatures than their glass transition temperatures. The crosslinking densities

Table 3
Penetration, interphase and total thickness of epoxy laminate samples.

Sample	Thickness		
	Penetration μm	Interphase μm	Total μm
D-H-110	14.5 ± 0.6	2.9 ± 0.3	17.4 ± 0.8
D-H-120	5.6 ± 0.5	2.9 ± 0.4	8.5 ± 0.5
D-H-140	3.5 ± 0.3	3.5 ± 0.4	6.9 ± 0.5
F-H-110	7.4 ± 0.5	2.5 ± 0.9	9.9 ± 0.5
F-H-140	2.6 ± 0.7	2.6 ± 0.6	5.2 ± 1.0

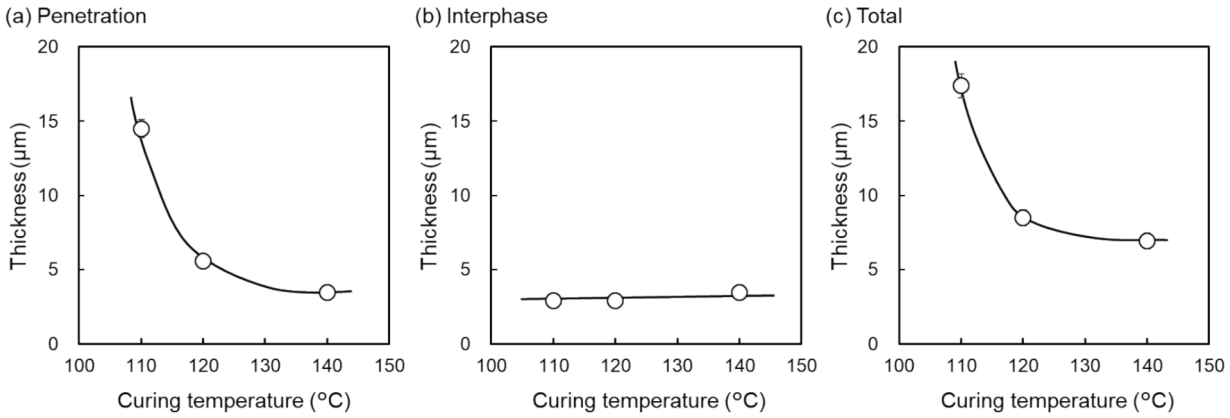

Fig. 4. (a) Penetration thickness, (b) interphase thickness and (c) total thickness of D-H-110, D-H-120 and D-H-140.

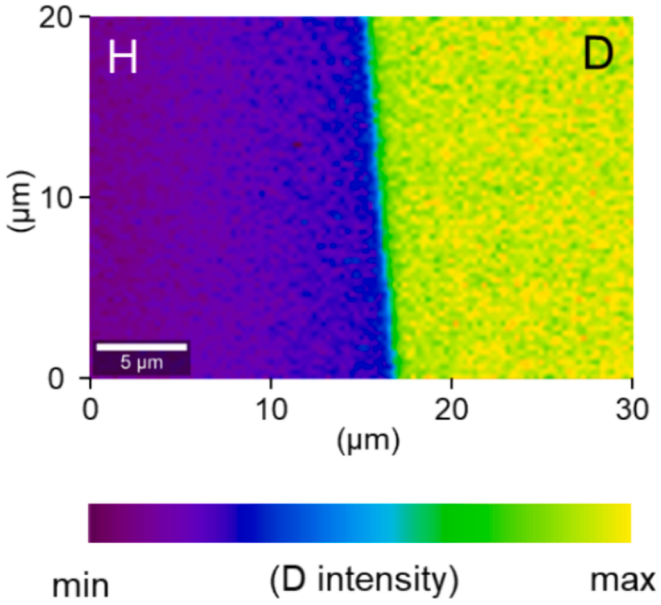

Fig. 5. Confocal Raman 2D mapping image of D-Epoxy/H-Epoxy interphase for D-H-110.

Table 4
Penetration, interphase and total thickness of H-Epoxy adhesion samples on F-Epoxy substrates.

Sample	Thickness		
	Penetration μm	Interphase μm	Total μm
H-F-110$_{\phi 100}$	9.6 ± 0.4	3.3 ± 0.4	12.9 ± 0.5
H-F-110$_{\phi 50}$	2.8 ± 0.2	3.4 ± 0.3	6.3 ± 0.2
H-F-110$_{\phi 0}$	1.1 ± 0.2	2.1 ± 0.4	3.1 ± 0.3
H-F-140$_{\phi 100}$	3.2 ± 0.3	3.2 ± 0.4	6.4 ± 0.6
H-F-140$_{\phi 50}$	1.5 ± 0.3	2.6 ± 0.3	4.2 ± 0.5
H-F-140$_{\phi 0}$	1.2 ± 0.4	2.3 ± 0.5	3.3 ± 0.3

ν of H-Epoxy-110, H-Epoxy-120 and H-Epoxy-140 were increased in this order as the curing temperature of H-Epoxy was raised. F-Epoxy-140 also possessed a higher ν value than F-Epoxy-110.

3.4. Mechanism of the formation of penetration and interphase regions

Fig. 6 shows the illustration of the crosslinking formation and the penetration of epoxy precursors into Epoxy-110 and Epoxy-140 substrates. As the above section was described, Epoxy-110 possessed lower crosslinking density, compared with Epoxy-140. In addition, The DSC results in Figure S4 in the Supplementary material supported that, regardless, the curing reactions of H-Epoxy and F-Epoxy have not completely progressed at 110 °C, whereas the curing reactions have almost completed at 140 °C. These mean the difference in crosslinking densities of the epoxy resins. It is suspected that the penetration behaviors of epoxy precursor adhesives depended strongly on the epoxy network structure, including the ν of the epoxy substrate, as shown in Fig. 6. Epoxy-110 has a lower ν than Epoxy-140, which enhanced the penetration behavior of the epoxy precursor. Therefore, Epoxy-110 has a larger penetration thickness.

In D-Epoxy/H-Epoxy laminates, the penetration thickness of D-H-110 was also larger than that of D-H-140. This result was coincident with H-Epoxy/F-Epoxy and F-Epoxy/H-Epoxy adhesion samples, which means that the penetration behaviors of D-Epoxy precursor were correlated to the ν values of the H-Epoxy substrates.

In our group, the correlation between adhesion properties and interphase thickness using crystalline polymer substrates has been reported previously [38,39]. Our previous studies revealed that the interphase structure depended on crystallization behaviors at interphase regions.

Herein, we focused on amorphous epoxy substrates and adhesives with thermoset network structures. Because the epoxy adhesives involved curing reaction of epoxy precursors by heating, the interphase region in epoxy/epoxy adhesion samples would be constructed due to the entanglement of polymer network and the penetration behavior of epoxy precursor molecules. Therefore, the molecular size of epoxy precursors and the network structure of the epoxy adherents had more significant effects on the penetration regions.

3.5. Adhesion test

In our previous work, the interphase structure and adhesion properties had a large correlation because the interphase was constructed by molecular diffusions and entanglements as well as crystal growing at the boundary regions [38,39]. In this study, we also focused on amorphous epoxy network structure at adhesion boundary regions and their adhesion properties. Although we performed the lap shear tests and peeling tests of their laminated samples, the substrates of all the samples were broken in their tests and the reliable adhesive strengths were not obtained. Therefore, we performed the wedge tests.

Fig. 7 and Table S1 in the Supplementary material shows the fracture toughness G_c by wedge tests and their penetration and interphase thicknesses.

For H-H-H wedge tests, the G_c values were 482 J/m^2, 43 J/m^2 and 38 J/m^2 for H-110, H-120 and H-140 substrates, respectively, and their penetration thicknesses were 14.5 μm, 5.6 μm and 3.5 μm, respectively.

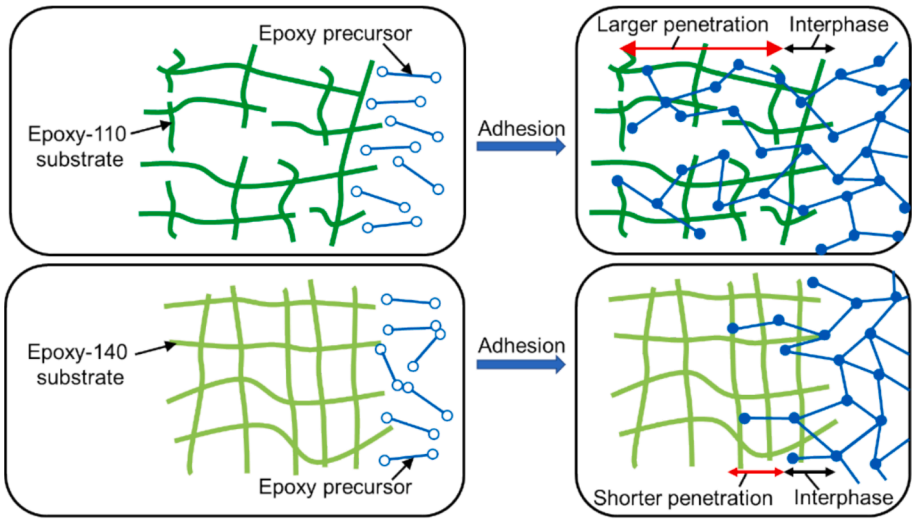

Fig. 6. Illustration of the crosslinking formation and penetration of the epoxy precursor for (upper) Epoxy-110 and (bottom) Epoxy-140 substrate.

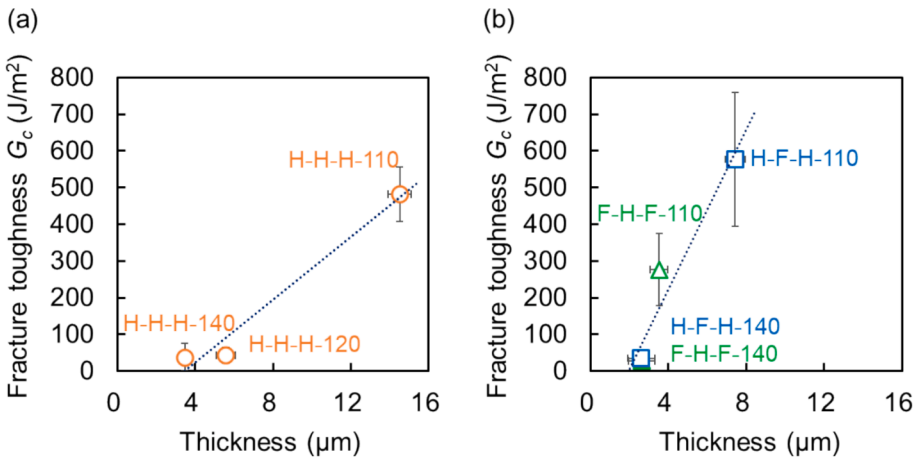

Fig. 7. Relationship between fracture toughness (G_c) and penetration thickness of (a) H-H-H, (b) H-F-H and F-H-F laminated samples.

The adhesion samples with H-110 substrates showed higher G_c values and larger penetration thickness than those with H-120 and H-140 substrates. These results indicated that the G_c values was decreased as the curing temperature of the adhered substrates increased from 110 °C to 140°C.

For H-F-H wedge tests, the G_c values were 576 J/m^2 and 35 J/m^2 for H-110 substrate and H-140 substrate, respectively. Their penetration thicknesses were 7.4 μm and 2.6 μm, respectively. For F-H-F wedge tests, the values of G_c were 276 J/m^2 and 28 J/m^2 for F-110 substrate and F-140 substrate, respectively, and their penetration thicknesses were 3.5 μm and 2.6 μm, respectively. H-F-H and F-H-F adhesion systems with H-110 and F-110 substrates also possessed higher G_c values and larger penetration thicknesses than those with substrates cured at 140 °C.

For the investigation on their fractural mode, the Raman spectroscopic measurements of the laminated surface after the H-F-H and F-H-F wedge tests were performed at several points. The measurement positions and their Raman spectra were shown in Figure S13 and S14 in the Supplementary material. In H-F-H-140, F-H-F-110 and F-H-F-110 laminates, one substrate side was composed of only H-Epoxy and the other was of F-Epopxy at the same position. In H-F-H-110 laminate, one substrate side was composed of only H-Epoxy and the other was of F-Epopxy including a slight amount of H-Epoxy. In the wedge tests of all the laminates, the propaegation of cracks would be progressed at the interphase region or near the interphase.

These results suggested that the correlation between G_c and penetration thicknesses. Since the substrates cured at 110 °C showed a lower v, the penetration behaviors of the epoxy precursors into these substrates were enhanced. These penetrations of epoxy precursors provided the larger penetration thickness, which directly resulted in the higher G_c.

4. Conclusions

We performed the investigation on the correlation between the structure of adhesion boundary and their fracture toughness of epoxy resin/epoxy resin adhesion systems. The analyses of the adhesion interphase with same or similar chemical components pose significant challenges because both polymers possess the same or similar chemical structure. In our study, the adhesion samples were composed of deuterated epoxy adhesives in the analyses of single-component adhesion boundary regions and fluorinated epoxy adhesives in the analyses of similar component boundary regions. We assessed to evaluate their boundary region structure by Raman scattering measurement using the labeled epoxy resins. It is proved that the boundary regions were divided into “penetration” and “interphase” regions. The laminates with larger penetration thickness possessed the larger fracture toughness. As the curing temperature of the substrates was increased from 110 °C to 140 °C or the molecular size of the epoxy precursor in adhesives was increased, the crosslinking densities of the substrates were increased and

penetration behaviors were prevented. These larger penetration thickness provided larger fracture toughness. These suggested that the procedure conditions of CFRP substrates also had a large impact on the adhesion properties, which strongly supported that the adhesion mechanism of "co-curing" system of CFRP was involving not only chemical bonds but also molecular diffusion and entanglements.

CRediT authorship contribution statement

Naho Aoki: Writing – review & editing, Writing – original draft, Visualization, Validation, Resources, Methodology, Investigation, Formal analysis, Data curation. **Junpei Yamazaki:** Data curation, Formal analysis, Methodology, Writing – original draft. **Takuya Matsumoto:** Writing – review & editing, Writing – original draft, Visualization, Validation, Supervision, Project administration, Methodology, Investigation, Formal analysis, Data curation, Conceptualization. **Masayasu Totani:** Writing – original draft, Methodology, Investigation, Formal analysis, Data curation. **Atsuomi Shundo:** Writing – review & editing, Writing – original draft, Investigation, Data curation. **Keiji Tanaka:** Writing – review & editing, Writing – original draft, Supervision, Project administration, Investigation, Formal analysis, Data curation. **Takashi Nishino:** Writing – review & editing, Supervision, Resources, Project administration, Methodology, Investigation, Funding acquisition, Formal analysis, Conceptualization.

Declaration of competing interest

The authors declare that they have no known competing financial interests or personal relationships that could have appeared to influence the work reported in this paper.

Data availability

No data was used for the research described in the article.

Appendix A. Supplementary data

Supplementary data to this article can be found online at https://doi.org/10.1016/j.compositesa.2024.108511.

References

[1] Soutis C. Fibre reinforced composites in aircraft construction. Prog Aerosp Sci 2005;41:143–51. https://doi.org/10.1016/j.paerosci.2005.02.004.

[2] Ma Y, Yang Y, Sugahara T, Hamada H. A study on the failure behavior and mechanical properties of unidirectional fiber reinforced thermosetting and thermoplastic composites. Compos B Eng 2016;99:162–72. https://doi.org/10.1016/j.compositesb.2016.06.005.

[3] Marsh G. Airframers exploit composites in battle for supremacy. Reinf Plast 2005;49:26–32. https://doi.org/10.1016/S0034-3617(05)00577-1.

[4] Zhang C, Zhang G, Xu J, Shi XP, Wang X. Review of curing deformation control methods for carbon fiber reinforced resin composites. Polym Compos 2022;43:3350–70. https://doi.org/10.1002/pc.26648.

[5] Liu L, Jia C, He J, Zhao F, Fan D, Xing L, et al. Interfacial characterization, control and modification of carbon fiber reinforced polymer composites. Compos Sci Technol 2015;121:56–72. https://doi.org/10.1016/j.compscitech.2015.08.002.

[6] Soutis C. Carbon fiber reinforced plastics in aircraft construction. Mater Sci Eng A 2005;412:171–6. https://doi.org/10.1016/j.msea.2005.08.064.

[7] Koronis G, Silva A, Fontul M. Green composites: a review of adequate materials for automotive applications. Compos B Eng 2013;44:120–7. https://doi.org/10.1016/j.compositesb.2012.07.004.

[8] Grant A. Sporting composites. Reinf Plast 2005;49:46–9. https://doi.org/10.1016/S0034-3617(05)70644-5.

[9] Mugahed Amran YH, Alyousef R, Rashid RSM, Alabduljabbar H, Hung C-C. Properties and applications of FRP in strengthening RC structures: a review. Structures 2018;16:208–38.

[10] Caminero MA, Lopez-Pedrosa M, Pinna C, Soutis C. Damage monitoring and analysis of composite laminates with an open hole and adhesively bonded repairs using digital image correlation. Compos B Eng 2013;53:76–91. https://doi.org/10.1016/j.compositesb.2013.04.050.

[11] Wang H, Zhang X, Duan Y. Effects of drilling area temperature on drilling of carbon fiber reinforced polymer composites due to temperature-dependent properties. Int J Adv Manuf Technol 2018;96:2943–51. https://doi.org/10.1007/s00170-018-1810-7.

[12] Soutis C, Curtis PT. Prediction of the post-impact compressive strength of cfrp laminated composites. Compos Sci Technol 1996;56:677–84. https://doi.org/10.1016/0266-3538(96)00050-4.

[13] Lee H, Ohsawa I, Takahashi J. Effect of plasma surface treatment of recycled carbon fiber on carbon fiber-reinforced plastics (CFRP) interfacial properties. Appl Surf Sci 2015;328:241–6. https://doi.org/10.1016/j.apsusc.2014.12.012.

[14] Zheng H, Zhang W, Li B, Zhu J, Wang C, Song G, et al. Recent advances of interphases in carbon fiber-reinforced polymer composites: a review. Compos B Eng 2022;233:109639. https://doi.org/10.1016/j.compositesb.2022.109639.

[15] Matsumoto T, Okumura Y, Ichimura M, Nakamura H, Honda K, Shibahara M, et al. Surface modification and adhesion mechanism of isotactic polypropylene with low-energy electron-beam treatments. Langmuir 2020;36:10846–52. https://doi.org/10.1021/acs.langmuir.0c01912.

[16] Nishida M, Hongo A, Takahara H, Higashide M. Effects of electron beam irradiation on hypervelocity impact behavior of carbon fiber reinforced plastic plates. J Compos Mater 2021;55:4295–304. https://doi.org/10.1177/00219983211037049.

[17] Yoo SH. Short review of utilization of electron-beam irradiation for preparing polyacrylonitrile-based carbon fibers and improving properties of carbon-fiber-reinforced thermoplastics. Carbon Letters 2022;32:413–29. https://doi.org/10.1007/s42823-021-00304-8.

[18] Tang L-G, Kardos JL. A review of methods for improving the interfacial adhesion between carbon fiber and polymer matrix. Polym Compos 1997;18:100–13. https://doi.org/10.1002/pc.10265.

[19] Yao SS, Jin FL, Rhee KY, Hui D, Park SJ. Recent advances in carbon-fiber-reinforced thermoplastic composites: a review. Compos B Eng 2018;142:241–50. https://doi.org/10.1016/j.compositesb.2017.12.007.

[20] Brauner C, Nakouzi S, Zweifel L, Tresch J. Co-curing behaviour of thermoset composites with a thermoplastic boundary layer for welding purposes. Adv Compos Lett 2020;29:2633366X20902777. https://doi.org/10.1177/2633366X20902777.

[21] Quan D, Zhao G, Scarselli G, Alderliesten R. Co-curing bonding of carbon fibre/epoxy composite joints with excellent structure integrity using carbon fibre/PEEK tapes. Compos Sci Technol 2022;227:109567. https://doi.org/10.1016/j.compscitech.2022.109567.

[22] Streitferdt A, Rudolph N, Taha I. Co-Curing of CFRP-steel hybrid joints using the vacuum assisted resin infusion process. Appl Compos Mater 2017;24:1137–49. https://doi.org/10.1007/s10443-016-9575-3.

[23] Quan D, Farooq U, Zhao G, Dransfeld C, Alderliesten R. Co-cured carbon fibre/epoxy composite joints by advanced thermoplastic films with excellent structural integrity and thermal resistance. Int J Adhes Adhes 2022;118:103247. https://doi.org/10.1016/j.ijadhadh.2022.103247.

[24] Studer J, Dransfeld C, Masania K. An analytical model for B-stage joining and co-curing of carbon fibre epoxy composites. Compos Part A Appl Sci Manuf 2016;87:282–9. https://doi.org/10.1016/j.compositesa.2016.05.009.

[25] Kawaguchi D, Nelson A, Masubuchi Y, Majewski JP, Torikai N, Yamada NL, et al. Precise analyses of short-time relaxation at asymmetric polystyrene interface in terms of molecular weight by time-resolved neutron reflectivity measurements. Macromolecules 2011;44:9424–33. https://doi.org/10.1021/ma201717e.

[26] Kotera M, Urushihara Y, Izumo D, Nishino T. Interfacial structure of all-polyethylene laminate using scanning thermal microscope and nano-Raman spectroscope. Polymer (Guildf) 2012;53:1966–71. https://doi.org/10.1016/j.polymer.2012.02.038.

[27] Shundo A, Yamamoto S, Tanaka K. Network formation and physical properties of epoxy resins for future practical applications. JACS Au 2022;2:1522–42. https://doi.org/10.1021/jacsau.2c00120.

[28] Aoki M, Shundo A, Yamamoto S, Tanaka K. Effect of a heterogeneous network on glass transition dynamics and solvent crack behavior of epoxy resins. Soft Matter 2020;16:7470–8. https://doi.org/10.1039/D0SM00625D.

[29] Prolongo SG, del Rosario G, Ureña A. Comparative study on the adhesive properties of different epoxy resins. Int J Adhes Adhes 2006;26:125–32. https://doi.org/10.1016/j.ijadhadh.2005.02.004.

[30] Pukánszky B. Interfaces and interphases in multicomponent materials: past, present, future. Eur Polym J 2005;41:645–62. https://doi.org/10.1016/j.eurpolymj.2004.10.035.

[31] Cognard J. The metal/polymer interphase in adhesive joints. Int J Adhes Adhes 1991;11:114–6. https://doi.org/10.1016/0143-7496(91)90036-H.

[32] Liu Y, Shigemoto Y, Hanada T, Miyamae T, Kawasaki K, Horiuchi S. Role of chemical functionality in the adhesion of aluminum and isotactic polypropylene. ACS Appl Mater Interfaces 2021;13:11497–506. https://doi.org/10.1021/acsami.0c22988.

[33] Horiuchi S, Liu Y, Shigemoto Y, Hanada T, Shimamoto K. In-situ TEM investigation of failure processes in metal-plastic joint interfaces. Int J Adhes Adhes 2022;117:103003. https://doi.org/10.1016/j.ijadhadh.2021.103003.

[34] Sharpe LH. The interphase in adhesion. J Adhes 1972;4:51–64. https://doi.org/10.1080/00218467208072210.

[35] Ajji A, Utracki LA. Interphase and compatibilization of polymer blends. Polym Eng Sci 1996;36:1574–85. https://doi.org/10.1002/pen.10554.

[36] Gentle TE, Schmidt RG, Naasz BM, Gellman AJ, Gentle TM. Organofunctional silanes as adhesion promoters: direct characterization of the polymer/silane interphase. J Adhes Sci Technol 1992;6:307–16. https://doi.org/10.1163/156856192X00359.

[37] Hartwig A, Meissner R, Merten C, Schiffels P, Wand P, Grunwald I. Mutual influence between adhesion and molecular conformation: molecular geometry is a

key issue in interphase formation. J Adhes 2013;89:77–95. https://doi.org/10.1080/00218464.2013.731363.
[38] Matsumoto T, Shimizu Y, Nishino T. Analyses of the adhesion interphase of isotactic polypropylene using hot-melt polyolefin adhesives. Macromolecules 2021;54:7226–33. https://doi.org/10.1021/acs.macromol.1c00647.
[39] Matsumoto T, Nakanishi Y, Hongo C, Hakukawa H, Horiuchi S, Nishino T. Adhesive interphase analyses of isotactic polypropylene and cyanoacrylate with cobalt complex primers. Polymer (Guildf) 2018;137:63–71. https://doi.org/10.1016/j.polymer.2018.01.011.
[40] Seong N-H, Fang Y, Dlott DD. Vibrational energy dynamics of normal and deuterated liquid benzene. J Phys Chem A 2009;113:1445–52. https://doi.org/10.1021/jp809679y.
[41] Ito M, Shigeoka T. Raman spectra of benzene and benzene-d6 crystals. Spectrochim Acta 1966;22:1029–44. https://doi.org/10.1016/0371-1951(66)80192-3.
[42] Huang J, Fu P, Li W, Xiao L, Chen J, Nie X. Influence of crosslinking density on the mechanical and thermal properties of plant oil-based epoxy resin. RSC Adv 2022;12:23048–56. https://doi.org/10.1039/D2RA04206A.
[43] Creton C, Kramer EJ, Hui CY, Brown HR. Failure mechanisms of polymer interfaces reinforced with block copolymers. Macromolecules 1992;25:3075–88. https://doi.org/10.1021/ma00038a010.
[44] Rocks J, Rintoul L, Vohwinkel F, George G. The kinetics and mechanism of cure of an amino-glycidyl epoxy resin by a co-anhydride as studied by FT-Raman spectroscopy. Polymer (Guildf) 2004;45:6799–811. https://doi.org/10.1016/j.polymer.2004.07.066.
[45] Damian CM, Vulcan MA, Zaharia A, Zaharia C, Vasile E, Iovu H. Advanced studies on synthesis and cure reaction of fluorinated epoxy resin. High Perform Polym 2016;28:1151–60. https://doi.org/10.1177/0954008315620288.